32nd Annual International Conference of the IEEE EMBS
Buenos Aires, Argentina, August 31 - September 4, 2010

Impedimetric Biosignal Analysis and Quantification in a Real-Time Biosensor System

Dean S. Messing, *Member, IEEE*, Andrey Ghindilis, and Kevin Schwarzkopf

***Abstract*— We describe our real-time, label-free, electrochemical impedance biosensor system with an emphasis on the use of an impedance response signal model to quantify assays. The signal processing for estimating model parameters from noisy data and the quantitative verification against target concentration and affinity are also presented.**

***Index Terms*— Label-free, affinity biosensor, nonlinear parameter estimation**

I. INTRODUCTION

An *affinity biosensor* is a device that can detect and assay specific *target* bio-molecules by using *probe* molecules immobilized on the biosensor surface. The probe is designed to bind both the surface and the desired target or *analyte*. The target is contained in a sample that might be a quantity of blood, water, air, or some other medium. The target bio-molecules might be a certain protein, DNA sequence, or other biochemical agent. Prior to use, such a biosensor must be *functionalised*. That is, its surface must be biochemically activated with *probe* molecules designed to specifically capture the target and, ideally, nothing else.

The operating principle of such a sensor can be viewed in three heuristic steps. First, the selective probe captures and binds target bio-molecules in the surrounding medium. Second, the target-probe complex induces changes in the sensor's surface properties that are correlated to the type and amount of bound target. Third, the changes are detected by some physical means that tracks the changes, and can be measured and analysed.

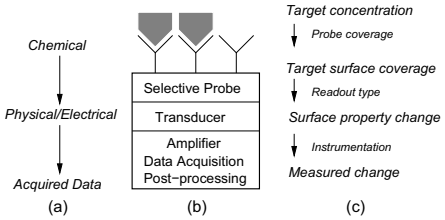

Fig. 1. General affinity biosensor: (a) Form of information (b) Physical sensor arrangement (c) Functional steps

Passage from the second to the third step is known as the *readout*. For example, a piezoelectric readout is the "transducer" found in many cantilever biosensors where the change in mass caused by target binding deforms a functionalised cantilever, which, in turn, induces change in a measurable electrical property due to the piezoelectric effect. A second readout example uses a fluorophore attached to the target molecule. The fluorescence due to bound target molecules is detected visually, or converted to a digital image for analysis. Yet another example is the impedimetric readout. Here, changes on the sensor surface induce (or, rather, transduce) a change in the impedance spectrum of the sensor treated as a one-port electrical component. All of these readout types use instrumentation to derive a signal from the readout to assay the target. These ideas are summarised in Fig. 1, taken from [1].

The majority of modern affinity biosensors are based on electrochemical or fluorescent detection of a molecular marker (label) attached to the target molecules. A labeled assay allows for substantial enhancement of the transducer signal compared to unlabeled methods, but it also requires additional stages of the assay work-flow, and complicates design of a real-time assay.

The well-established impedimetric approach requires no molecular markers for detection and thus holds great potential for the development of real-time and label-free affinity biosensors. It is therefore currently gaining in importance due to the simplicity of the assay procedure and the possibility of characterising the analyte binding kinetics.

In previous work [2] we used an impedimetric biosensor array for specific detection of target DNA molecules. We have since developed a new configuration for the sensor array and a technology for its bio-functionalisation. In addition, stimulus/acquisition instrumentation, and signal processing algorithms for impedimetric signal analysis were developed. This paper focuses on these last two items.

The paper is organised as follows. Section II describes, in general terms, the electrical operation of the sensor. Section III provides a high-level description of the stimulus/acquisition system. Significant development challenges of this new system are related to the creation of mathematical algorithms for (i) system stimulation and control,[1] and (ii) analysis of the captured noisy impedimetric signal in order to correlate its parameters to the target-to-probe binding kinetics. In section IV, we discuss (ii) where we present a signal model based on surface chemistry, and a spectral estimation algorithm from the field of NMR signal processing [3] to estimate the model parameters.

II. IMPEDANCE BIOSENSOR

The heart of the electrochemical impedance biosensor system is the *interdigitated electrode* (IDE). Fig. 2(a) shows a complete sensor die with fifteen electrodes. Fig. 2(b) is

All authors are with Sharp Laboratories of America, 5750 NW Pacific Rim Blvd, Camas, Washington, 98607, USA.
Corresponding author e-mail: deanm@sharplabs.com

[1] for the purpose, for example, of on-chip real-time PCR.

a micrograph of one group of electrodes. Fig. 2(d) depicts one channel of the IDE as a one-port linear device, $\mathfrak{L}$, driven by stimulus voltage $v(t)$, and having response current $i(t)$. Impedance is strictly defined only when the voltage-

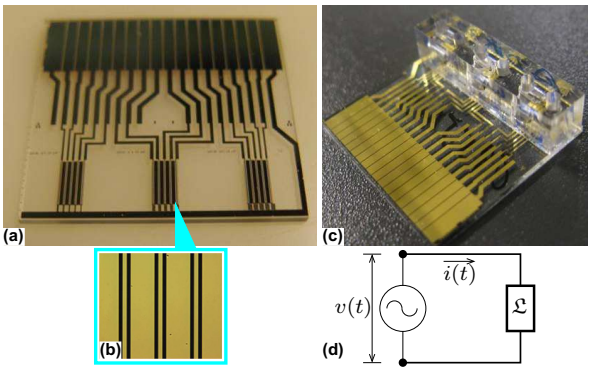

Fig. 2. **(a)**: Sensor die. **(b)**: Micrograph of electrode. **(c)**: 15-channel sensor array with attached microfluidic chambers. **(d)**: One-port linear circuit.

current relationship is linear. A constant amplitude sinusoidal function of time $v(t)$ gives rise to sinusoidal $i(t)$. Formally,

$$\begin{aligned} v(t) &= V\cos(2\pi ft-\theta) \\ i(t) &= I(f)\cos(2\pi ft-\varphi(f)), \end{aligned}$$

where V and f are the amplitude and frequency of the stimulus voltage, θ its phase, and $I(f)$ and $\varphi(f)$ the amplitude and phase of the response current. Both I and φ generally vary with the stimulus frequency.

One definition [4] of the complex impedance of $\mathfrak{L}$ as a function of frequency is the ratio of the phasors that represent $v(t)$ and $i(t)$ respectively:

$$Z(f)=\frac{V}{I(f)}e^{j(\varphi(f)-\theta)},\quad (j:=\sqrt{-1}).$$

For simplicity we henceforth suppress the dependence on f and assume $\theta=0$. Thus, in polar form, $Z=(V/I)\angle\varphi$.

Near-linear operation of the sensor during bio-reactions is achieved by keeping the driving voltage small [5]. Typically V does not exceed 150 mv. Small V (and no DC bias voltage) has the additional benefit of inhibiting unwanted redox.

III. SYSTEM DESCRIPTION

This section describes the stimulus-transduction-acquisition system. The functional diagram is depicted by everything other than the *Laptop Computer* in Fig. 3.

The signal chain begins on the left with Stimulus Generation. This is performed by an off-the-shelf direct digital synthesiser (DDS) and built-in D/A converter. The DDS frequency, f, is under the control of a μ-processor controller (grey arrow) which, in turn, receives f from either the user interface or a programmed frequency control algorithm running on the laptop. The latter is for computation of the impedance spectrum across a band of frequencies. The DDS is also capable of multi-tone stimulus.

The biosensor transducer consists of an array of fifteen electrodes separated into three groups of five. Each group is sealed in a microfluidic chamber schematically shown in Fig. 3 by blue rectangles labeled *Cell 0*, *Cell 1*, and *Cell 2*. Fig. 2(c) shows the 15-channel array with attached microfluidic chambers.

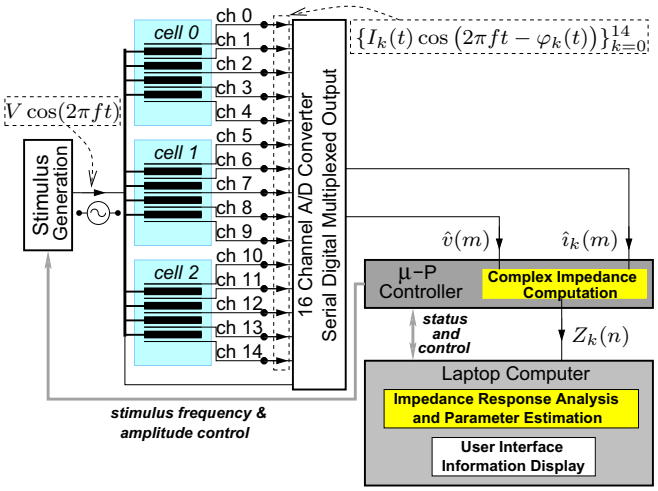

Fig. 3. Biosensor system functional block diagram.

All electrodes are stimulated in parallel by $v(t)$. Along with $v(t)$, the fifteen response currents, $\{i_k(t)\}_{k=0}^{14}$, are sampled in parallel by the 16-channel A/D converter and multiplexed onto a serial digital connection to the μ-processor for impedance calculation. Not shown are multi-gain linear amplifiers that buffer $i_k(t)$ and $v(t)$ before sampling. For frequencies below 75 Hz, the amplitude of $i_k(t)$ becomes small and additional amplification is required. Amplifier gains are under μ-processor control so that an optimal signal-to-noise ratio can be maintained across a range of frequencies and over the dynamic range of the converter.

The A/D outputs, $\hat{v}(m)$ and $\hat{i}_k(m)$, are the sampled voltage and current signals. Impedance is computed from these as discussed below. The computation is presently done within the μ-processor firmware, but it could just as well be done by the laptop if access to $v(m)$ and $i_k(m)$ is desired. The complex impedance response profiles, $\{Z_k(n)\}_{k=0}^{14}$, are then passed to the laptop for analysis and parameter estimation.

Blocks in Fig. 3 responsible for signal processing are coloured yellow. The first of these is the algorithm that derives $Z_k(n)=|Z_k(n)|\angle\varphi(n)$ from $\hat{v}(m)$ and $\hat{i}_k(m)$. The two time indices, m and n, indicate that $Z_k(n)$ is sampled at a different (lower) rate than $\hat{v}(m)$ and $\hat{i}_k(m)$.

A. Impedance Calculation

We use a Fourier Domain scheme for calculating impedance. The sampled stimulus voltage and response current are transformed into the Fourier Domain using a windowed (short-time) Discrete-time Fourier Transform (DTFT) tuned to the stimulus frequency. This presents no computational burden on the laptop because the impedance is only computed every 125 ms.

Values of the phasor voltage and current obtained from the DTFT are only approximate due to the interference between the complex Fourier components of a sinusoid that has been time-limited. This is especially true at low frequencies

where just one or two cycles plus a fraction are included in the short-time window. It is therefore necessary to apply a correction scheme to get impedance values uncorrupted by the window. The algorithm yields corrected phasors $Ve^{j\theta}$ and $I(n)e^{j\varphi(n)}$ from which complex impedance is derived as discussed in section II. The sampling index n represents the center of the short-time window over which $Z(n)$ is computed.

B. Operational Results [2]

In the following discussion we focus on the behaviour of the *magnitude* of the complex impedance, $|Z_k(n)|$, and not its phase. These results were gathered using a relatively low stimulus frequency (75 Hz) at which the phase changes little during target binding.

Figure 4(a) shows an example of the operation of the system described above. The example involves the difference between the responses of F11 E. coli single-stranded DNA (ssDNA) and F24 E. coli ssDNA when all sensors are functionalised to select F11.

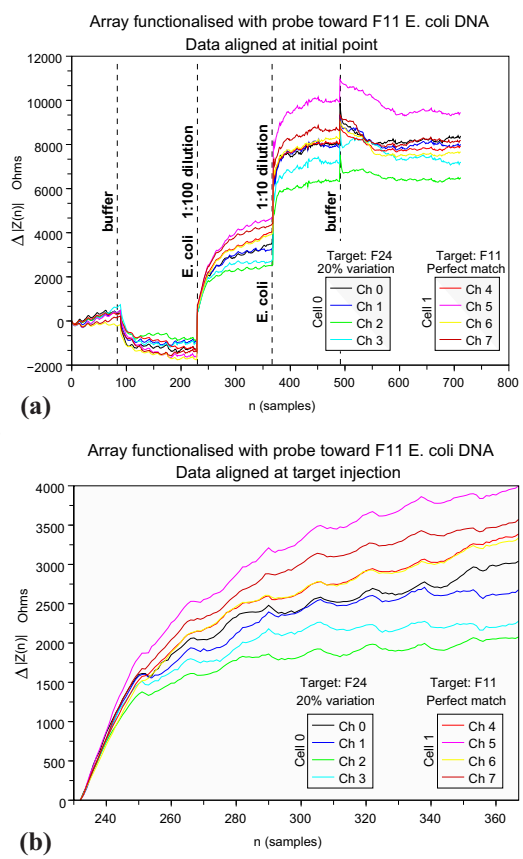

Fig. 4. **(a)**: Responses of the eight multiplexed sensors functionalised to select F11 E. coli ssDNA. In Cell 0, F24 ssDNA was injected, whose nucleotide sequence varies by 20% compared to F11. In Cell 1, F11 was injected. **(b)**: Zoom of the interval-of-interest between injection of 1:100 dilution target and 1:10 dilution target.

Fig. 4(a) was obtained by acquiring $\{|Z_k(n)|\}_{k=0}^{7}$ after null buffer solution was injected into the cells. The signal variation between $n = 0$ and about $n = 90$ samples is due to poorly understood [1] random electronic and biochemical *drift*. Another injection of buffer occurred at about $n = 90$ samples, roughly six minutes into the acquisition. A target with dilution in the ratio of 1:100 was injected at about $n = 230$. Higher concentration target, diluted in the ratio of 1:10, was then injected at about $n = 370$. Our *analysis aperture* lies between these two events, a duration of nine minutes. From this interval a mathematical algorithm will estimate signal parameters as discussed section IV. A final injection of buffer at about $n = 490$ produces an *elution* response which might be used to estimate additional kinetic information such as disassociation rate.

Two E. coli ssDNA variants, referred to as F11 and F24, were involved in the experiment. All eight sensors (four in each cell)[2] were functionalised with a probe designed for specific binding with an F11 target. A sample with F11 ssDNA was injected into Cell 1 of the array. Thus, the sensor responses obtained from Cell 1 correspond to a perfect match between target and probe. On the other hand, a sample containing F24 ssDNA was injected into Cell 0 of the same array. Its nucleotide sequence contained 5 mismatches (20% of the binding sequence) relative to the probe. Thus we expect F24 to have a lower affinity for the probe than F11. Fig. 4 suggests that the F24 variant target does appear to have lower affinity than F11. This is seen in Fig. 4(b) from the impedance profiles of Cell 0 (20% mismatch) falling somewhat below those of Cell 1 (perfect match).

Although the group of profiles from Cell 0 are visually distinguishable from those of Cell 1, it is nonetheless difficult to draw quantitative conclusions about the difference in affinity because the profiles are not well-separated. In addition, although the concentrations of F11 and F24 were nominally the same, their actual values may have differed significantly due to the inaccuracies of DNA target quantification and pipetting error. This further confounds the interpretation of the curves because both concentration and affinity affects the rate of increase. Finally, a common means within the bio-analytical community of drawing conclusions from such profiles is by fitting a line to the first few sample to estimate the *initial slope* of the response [2]. But Fig. 4(b) shows that the initial slopes of the eight profiles are nearly the same, making simple line-fitting approaches inadequate.

A more sophisticated mathematical approach is therefore needed to quantify signal parameters relevant to the bio-process. The next section outlines algorithms that we have investigated to estimate useful quantitative information from impedance response profiles.

IV. SIGNAL PROCESSING

A. Signal Model

Surface chemistry theory predicts that target molecules bind to the immobilised probe layer at a rate that obeys an exponential function[3] that decreases with time after the

[2]Results in this section were obtained with an older 8-channel sensor array organised into two cells of four channels each, as reflected in the discussion, Fig. 4, and Fig. 7.

[3]This behaviour is governed by the *Langmuir Adsorption Isotherm* which describes surface binding for sites that are identical and non-interacting.

target is injected into the microfluidic chamber. The bound target induces a change in the electrical characteristics at the boundary[4] of the liquid and sensor surface. This is manifested by a time-varying change in the measured impedance at fixed frequencies. This function of time, or sample index n in the discrete-time case, is well-modeled by

$$|Z(t)| = B + A(1 - e^{-\alpha t}) + \nu(t), \qquad (1)$$

where $\alpha, A, B \geq 0$ are constants.

Here, B is the constant offset at which the exponential begins, and represents the biosensor baseline impedance of the buffer solution (ignoring drift) prior to target injection. The noise inherent in every biosensor is represented by ν. Shown in blue in Fig. 5 is a typical noisy impedance signal

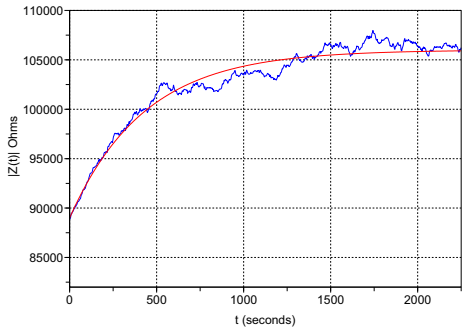

Fig. 5. Typical noisy impedance signal (blue) and impedance model function without noise (red).

during target binding. An estimation algorithm takes such a signal as input and estimates the exponential time constant, α, the amplitude, A, and the offset, B. From these an estimate of the underlying model function can be computed from Eq. 1. An example model function is shown by the red curve in Fig. 5.

Both α and A hold important biochemical information. The former closely tracks the concentration of the analyte, and the latter the sensor surface coverage, which is correlated to molecular affinity.

B. Non-linear Estimation Algorithms

The chief difficulties in estimating the parameters of Eq. 1 are the substantial additive noise present in the signal and the non-linear involvement of α.

We investigated methods for performing non-linear estimation that belong to an algorithm class having several common features. First is an assumed general signal model composed of uniformly spaced samples of a sum of M complex exponentials corrupted by zero-mean Gaussian noise, $\nu(n)$, and observed over a time aperture of N samples. This is described by the formula

$$y(n) = \sum_{k=1}^{M} a_k e^{\beta_k n} + \nu(n) \quad n = 0, 1, \ldots, N-1. \qquad (2)$$

[4]The *double-layer*, a buildup of excess ions of opposite charge to the local electrode surface, exists at this boundary and is responsible for the majority of the changing impedance.

The $\{\beta_k\}$ are called the *complex frequencies* or *poles* of the signal and $\{a_k\}$ are the complex amplitudes. Here $\beta_k = -\alpha_k + j2\pi f_k$ are complex numbers ($\alpha_k \geq 0$). The $\{\alpha_k\}$ are the pole damping factors and $\{f_k\}$ are the pole frequencies. It is clear that Eq. 1 is a special case of Eq. 2, with two real poles (one of which at the origin of the complex plane) and real-valued amplitudes $(B + A)$ and $-A$.

Second, the non-linear problem is broken into two steps [6]. Step 1 uses the *linear prediction* property, $y(n) = \sum_{k=1}^{M} c_k y(n-k)$, of Eq. 2 (with $\nu = 0$) to perform the simpler task of estimating parameters of a related linear model. Step 2 then extracts the non-linear parameters from the linear model.

The last common feature is that Step 1 employs a low dimensional subspace projection of the matrix associated with the linear model to reduce the effects of noise.

Two algorithm families within this class were investigated. The first family is typified by the Kumarisan-Tufts method described in [7]. In these approaches, Step 1 designs an adaptive (linear) filter that nulls any input signal of the form of Eq. 2. Step 2 extracts the zeros of the filter polynomial and computes the $\{\beta_k\}$ via algebraic manipulation of each zero. Following this, a scheme such as *Total Least Squares* is used on the partial model to estimate the $\{a_k\}$.

The second family of approaches uses a state-space representation for the linear model. Step 1 uses the input data to estimate the parameters of the state-feedback matrix associated with a related linear model. The eigenvalues of the matrix, which contain the system poles of Eq. 2, are computed in Step 2. The remainder of Step 2 (i.e., estimating the $\{a_k\}$) is as above.

A promising technique was found in a state-space NMR signal processing algorithm due to Fotinea, et al., described in [3]. Results in the next subsection were obtained using an adaptation of this approach for the biosensor system.

C. Signal Processing Results

In addition to extensive testing with synthetic signals, we verified the estimation algorithm using a titration series of five dilutions of (asP2P5) oligonucleotide ranging from 0.324–5 μM. We were interested in the variation of the estimated time constant, α. Fig.6(a) shows the results of estimating α for each molar concentration used (blue points). We note that four of the five points lie nearly on a straight line, the expected behaviour predicted by the Langmuir Isotherm. Deviation from the line by the last point may be due to factors such as *steric hindrance* there occur at high concentrations. In any case, normal operation of the Biosensor would use a calibration curve relating α to concentration so that such deviations would be compensated.

Fig.6(b) shows the response of the lowest concentration assay and the estimated model curve (in red) computed in the analysis aperture during target binding.

We also applied the algorithm to the E. coli data of Fig. 4. The data records were especially short (138 samples) and substantial periodic interference polluted the data due to a mal-adjusted temperature controller. Nonetheless

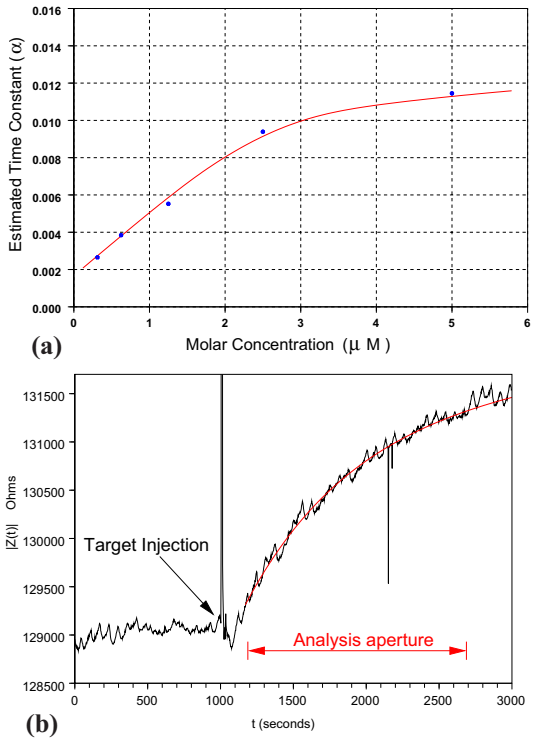

Fig. 6. **(a)**: Results of algorithmic analysis of titration series impedance responses using 5 concentrations of (asP2P5) oligonucleotide. **(b)**: Impedance response from lowest concentration (325 nM) response is shown in black. Model curve is shown in red.

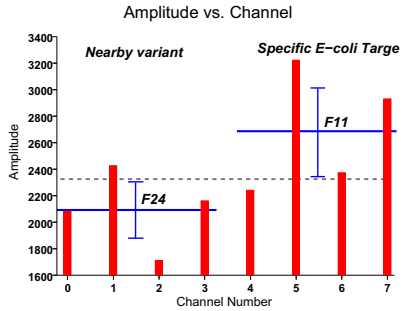

Fig. 7. Estimated response amplitude (A in Eq. 1) plotted again channel. Channels 0–3 correspond to Cell 0 (F24 ssDNA) and channels 4–7 to Cell 1 (F11 ssDNA).

the algorithm was able to disambiguate the F11 and F24 results as shown in Fig. 7 where the estimated amplitude is plotted against channel number. The mean values of the four channels in each of the two cells is indicated by the blue horizontal bars. It is easy to see that the mean amplitudes are well separated. Ninety-five percent confidence intervals are shown for each mean value.

V. CONCLUSION

We have presented a high-level description of a real-time Impedance Biosensor System. Two species of E. coli ssDNA whose nucleotide sequences differed by just 20% were used to demonstrate that nearby variants were distinguishable through signal analysis of the impedance responses, whereas visual inspection of the responses was ambiguous.

The technology for the analysis is a non-linear parameter estimation algorithm based on a Signal Model derived from surface chemistry. The algorithm enables quantification of impedimetric biosignals in terms of meaningful biochemical parameters such as concentration and affinity that are well-correlated to the Model. We estimated model parameters for both a titration series and the two E. coli species. The former showed correct behaviour against measured concentration, and the latter showed that the E. coli species were numerically distinguishable based on binding affinity.

VI. SOME FUTURE DIRECTIONS

The estimation algorithm discussed in section IV-B applies to a wide range of label-free real-time assay types including single nucleotide polymorphism, genotyping, low affinity ligand-receptor binding, and immunoassay.

The algorithm lends itself to variable size data sets so that fast, early parameter estimates are available, which become refined as more data is acquired.

Discrimination of specific target binding response from non-specific is one of the major challenges for label-free assay techniques. Along with biochemical approaches that aim at minimising non-specific binding, the estimation algorithm has the potential to discriminate two or more signals and thus separate specific from non-specific binding.

Finally, the estimation algorithm coupled with addition to the system of numerically controllable microfluidics holds potential for detailed characterisation of binding events, and thus increased selectivity.

VII. ACKNOWLEDGMENTS

The authors gratefully acknowledge the contribution by *The Center for Coastal Margin Observation & Prediction* of the bio-products used in the E. coli experiment.

REFERENCES

[1] Jonathan S. Daniels and Nader Pourmand, "Label-free impedance biosensors: Opportunities and challenges," *Electroanalysis*, vol. 19, no. 12, pp. 1239–1257, May 2007.

[2] Andrei L. Ghindilis, Maria W. Smith, Kevin R. Schwarzkopf, Changqing Zhan, David R. Evans, António M. Baptista, and Holly M. Simon, "Sensor array: Impedimetric label-free sensing of dna hybridization in real time for rapid, pcr-based detection of microorganisms," *Electroanalysis*, vol. 21, no. 13, pp. 1459–1468, 2009.

[3] Stavroula-Evita Fotinea, Ioannis Dologlou, and George Carayannis, "On the use of decimation for efficient spectral estimation," *Int'l. J. Computer Maths. & Appl. (HERMIS-μπ)*, vol. 8, pp. 84–100, Oct. 2006.

[4] Charles A. Desoer and Erest S. Kuh, *Basic Circuit Theory*, McGraw-Hill Book Co., New York, 1969.

[5] G. Barbero, A. L. Alexe-Ionescu, and I. Lelidis, "Significance of small voltage in impedance spectroscopy measurements on electrolytic cells," *J. Appl. Phys*, vol. 98, no. 11, 2005.

[6] Bhaskar D. Rao and K. S. Arun, "Model based processing of signals: A state space approach," *Proceedings of the IEEE*, vol. 80, no. 2, pp. 283–309, Feb. 1992.

[7] Ramdas Kumaresan and Donald W. Tufts, "Estimating the parameters of exponentially damped sinusoids and pole-zero modeling in noise," *IEEE Trans. Acous. Speech, Sig. Proc.*, vol. 30, no. 6, pp. 833–840, Dec. 1982.